Clinical Trial with Sodium ^{99m}Tc-Pertechnetate Produced by a Medium-Energy Cyclotron: Biodistribution and Safety Assessment in Patients with Abnormal Thyroid Function

Svetlana V. Selivanova[1,2], Éric Lavallée[1], Helena Senta[1], Lyne Caouette[1], Alexander J.B. McEwan[3], Brigitte Guérin[1,2], Roger Lecomte[1,2], and Éric Turcotte[1,2]

[1]Sherbrooke Molecular Imaging Center, CRCHUS, Sherbrooke, Quebec, Canada; [2]Department of Nuclear Medicine and Radiobiology, Faculty of Medicine and Health Sciences, Université de Sherbrooke, Sherbrooke, Quebec, Canada; and [3]Cross Cancer Institute, Edmonton, Alberta, Canada

A single-site prospective open-label clinical study with cyclotron-produced sodium ^{99m}Tc-pertechnetate (^{99m}Tc-NaTcO$_4$) was performed in patients with indications for a thyroid scan to demonstrate the clinical safety and diagnostic efficacy of the drug and to confirm its equivalence with conventional ^{99m}Tc-NaTcO$_4$ eluted from a generator. **Methods:** ^{99m}Tc-NaTcO$_4$ was produced from enriched ^{100}Mo (99.815%) with a cyclotron (24 MeV; 2 h of irradiation) or supplied by a commercial manufacturer (bulk vial eluted from a generator). Eleven patients received 325 ± 29 (mean ± SD) MBq of the cyclotron-produced ^{99m}Tc-NaTcO$_4$, whereas the age- and sex-matched controls received a comparable amount of the generator-derived tracer. Whole-body and thyroid planar images were obtained for each participant. In addition to the standard-energy window (140.5 keV ± 7.5%), data were acquired in lower-energy (117 keV ± 10%) and higher-energy (170 keV ± 10%) windows. Vital signs and hematologic and biochemical parameters were monitored before and after tracer administration. **Results:** Cyclotron-produced ^{99m}Tc-NaTcO$_4$ showed organ and whole-body distributions identical to those of conventional ^{99m}Tc-NaTcO$_4$ and was well tolerated. All images led to a clear final diagnosis. The fact that the number of counts in the higher-energy window was significantly higher for cyclotron-produced ^{99m}Tc-NaTcO$_4$ did not influence image quality in the standard-energy window. Image definition in the standard-energy window with cyclotron-produced ^{99m}Tc was equivalent to that with generator-eluted ^{99m}Tc and had no particular features allowing discrimination between the ^{99m}Tc production methods. **Conclusion:** The systemic distribution, clinical safety, and imaging efficacy of cyclotron-produced ^{99m}Tc-NaTcO$_4$ in humans provide supporting evidence for the use of this tracer as an equivalent for generator-eluted ^{99m}Tc-NaTcO$_4$ in routine clinical practice.

Key Words: sodium ^{99m}Tc-pertechnetate; cyclotron; thyroid imaging; safety; efficacy

J Nucl Med 2017; 58:791–798
DOI: 10.2967/jnumed.116.178509

Received Jun. 9, 2016; revision accepted Sep. 13, 2016.
For correspondence or reprints contact: Svetlana V. Selivanova, CIMS, CRCHUS, 3001, 12th Avenue Nord, Sherbrooke, Quebec J1H 5N4, Canada.
E-mail: Svetlana.V.Selivanova@USherbrooke.ca
Published online Oct. 13, 2016.

Despite a steady increase in procedures with PET, the role of ^{99m}Tc in nuclear imaging remains important, and frequent use of this tracer will continue well into the future (*1*). At the same time, the conventional supply chain for ^{99m}Tc is currently fragile because of aging nuclear reactors and the transition from the use of highly enriched uranium to the use of low-enriched uranium in targets for nuclear reactors. In addition, full-cost recovery for the production of medical isotopes promises to increase the prices for ^{99}Mo/^{99m}Tc generators, rendering alternative technologies for the production of medical isotopes more competitive (*2*). The direct production of ^{99m}Tc by cyclotrons is a decentralized approach that could satisfy the demand for ^{99m}Tc on a regional level (*3*) and help alleviate the low supply of ^{99m}Tc.

The production of ^{99m}Tc via proton irradiation of enriched ^{100}Mo results in the coproduction of several ^{9x}Tc radionuclides. Hence, the safety and imaging characteristics of cyclotron-produced ^{99m}Tc must be assessed for any unanticipated adverse effects. The first clinical trial demonstrated that cyclotron-produced ^{99m}Tc-pertechnetate obtained at 17 MeV was safe in humans (*4*). Theoretic (*5*) and empiric (*6*) analyses showed that the ^{99m}Tc production yield doubled when incident energy increased from 16 to 24 MeV. However, the radionuclidic purity greatly depended on the irradiation conditions, in particular, on the incident proton beam energy and irradiation time (*6,7*).

To take advantage of the higher production capacity of medium-energy cyclotrons, we first investigated the quality of ^{99m}Tc produced at 24 MeV. Its chemical and radiochemical purity as well as patient dosimetry were shown to be suitable for human use (*7*). A prospective open-label clinical study with sodium ^{99m}Tc-pertechnetate (^{99m}Tc-pertechnetate; ^{99m}Tc-NaTcO$_4$) prepared from a cyclotron at 24 MeV was initiated in patients with indications for a thyroid scan to demonstrate the clinical safety and diagnostic efficacy of the radiopharmaceutical and to confirm its utility in clinical procedures (ClinicalTrials.gov identifier: NCT02307175; approved by Health Canada). The images were analyzed qualitatively and quantitatively and compared with those obtained with conventional ^{99m}Tc-pertechnetate eluted from a generator.

MATERIALS AND METHODS

Provision of ^{99m}Tc-Pertechnetate

^{99m}Tc was produced on-site with a TR-24 cyclotron (Advanced Cyclotron Systems, Inc.) by irradiation of enriched ^{100}Mo (99.815%; 0.17%

TABLE 1
Radioisotopic Composition of Cyclotron-Produced ($24 \rightarrow 19 \pm 1$ MeV, 2 h) ^{99m}Tc-Pertechnetate at EOB

Nuclide*	Half-life (h)	γ-ray energy (keV)	Content†
^{99m}Tc	6.015	140.511	99.979 ± 0.009
^{97m}Tc	2,184	96.5	0.0006 ± 0.0001
^{96}Tc	102.7	812.54	0.013 ± 0.007
^{95}Tc	20	765.789	0.0017 ± 0.0003
^{95m}Tc	1,464	582.082	0.000008 ± 0.000005
^{94}Tc	4.9	702.67	0.0023 ± 0.0004
^{93}Tc	2.75	1,362.94	0.0032 ± 0.0004

*Physical properties are from Brookhaven National Laboratory National Nuclear Data Center (nuclear structure and decay data; NuDat 2.5; 2011; http://www.nndc.bnl.gov/nudat2).

†Measured by γ-ray spectrometry and reported as percentages (*7*).

^{98}Mo; 0.003% each ^{92}Mo−^{97}Mo) at 24 MeV for 2 h as described previously (*7*). The targets were processed to recover an effective thickness corresponding to an energy loss of approximately 5 MeV. Extraction of ^{99m}Tc was performed following a published procedure (*7*) that was a modification of another procedure (*8*). Quality control of the formulated ^{99m}Tc-pertechnetate solution for injection was done for all prepared batches in accordance with previously described standard procedures (*7*). The endotoxin levels were assayed by the *Limulus* amebocyte lysate method with an Endosafe-PTS test system (Charles River Laboratories International, Inc.). Sterility tests were performed by a licensed laboratory (Nucro-Technics). Generator-eluted ^{99m}Tc was supplied by Isologic Innovative Radiopharmaceuticals.

Study Design

This single-site prospective nonrandomized case–control open-label study included 19 patients who were referred to the nuclear medicine department with indications for a thyroid scan. The study was approved by the institutional ethics committee and by Health Canada. Each patient signed an approved written informed consent form. The recruited patients had thyroid disease (hyperthyroidism or thyroid nodule assessment), were 18−80 y old, had biochemical parameters within normal limits for their ages, and had a Karnofsky performance status of greater than 50%. Eleven recruited participants were administered cyclotron-produced ^{99m}Tc-NaTcO$_4$ (340 MBq ± 10%). Eight participants were paired by sex and age (±1 y) with the first group and were administered the same amount of ^{99m}Tc-NaTcO$_4$ supplied commercially (eluted from a generator) to serve as a control cohort. All participants underwent a prescribed thyroid imaging procedure and an additional whole-body scan.

Safety Monitoring

Safety was assessed by monitoring vital signs, biochemical laboratory test results, and adverse events at various time points during the study. On the day of the procedure, the participants were examined by a physician. Physical examination included the lungs, heart, vascular system, lymph nodes, and skin and a neurologic assessment. Vital signs (body temperature, blood pressure, heart rate, and respiratory rate), electrocardiogram, and oxygen saturation level were monitored before and after tracer administration. Blood samples were collected for hematologic and biochemical tests (complete blood count with differential and comprehensive metabolic panel) before and after tracer administration. Adverse events were monitored during the procedure and up to 24 h after the procedure. Participants were enrolled sequentially when no adverse events were reported by previous participant.

Estimation of Internal Radiation Dose

Estimation of the internal radiation dose for each patient was based on the amount of each technetium radioisotope present in the radiopharmaceutical preparation at the time of intravenous administration. The calculations were performed as described elsewhere (*7*), and the obtained values were compared with the predicted dose increase (*7*).

Image Acquisition

Thyroid images were acquired for 10 min in the planar mode with an Infinia Hawkeye 4 SPECT/CT camera (GE Healthcare) equipped with a 3-mm pinhole collimator (image matrix, 256 × 256). After thyroid imaging, anterior and posterior whole-body planar projections (4 or 5 bed positions; 3 min each) were acquired with a Discovery NM/CT 670 SPECT/CT camera (GE Healthcare) equipped with low-energy high-resolution collimators (image matrix, 256 × 1,024). For whole-body imaging, data were acquired in lower-energy (117 keV ± 10%) and higher-energy (170 keV ± 10%) windows in addition to the standard-energy (140.5 keV ± 7.5%) window.

Image Analysis: Biodistribution and Quality Evaluation

Qualitative image analysis based on visual interpretation was performed to compare the biodistributions of ^{99m}Tc-pertechnetate produced by both methods. Two nuclear medicine specialists were asked to rate the uptake as absence of uptake, light uptake, or intense uptake in the brain, thyroid, salivary glands, heart blood pool, lungs, liver, stomach, kidneys, bladder, soft tissues, and bone. Next, the interpreters were asked to rate the biodistribution of ^{99m}Tc-pertechnetate as normal or abnormal, taking into account the presence of specific diseases that may modify the biodistribution (e.g., complete thyroid resection explaining the absence of thyroid uptake or gastric hiatal hernia indicating mediastinal uptake). For the evaluation of image quality, both nuclear medicine specialists were shown the images randomly and were asked to tentatively discriminate between ^{99m}Tc-pertechnetate production methods.

For the quantitative evaluation of possible interference due to scatter from high-energy isotopic impurities, the geometric means of the raw count data from the anterior and posterior whole-body projections in each acquisition were computed for the standard-, lower-, and higher-energy windows. The ratios of the geometric mean counts in the lower-energy window and the higher-energy window to those in the standard-energy window were then calculated and compared for the cyclotron- and generator-produced radiotracers.

Statistics

Blood test results, biochemical test results, and vital signs were compared before and after ^{99m}Tc-pertechnetate injection with a Wilcoxon matched-pairs signed rank test. Results with P values of less than 0.05 were considered significant and clinically significant when outside normal physiologic limits.

Phantom Imaging

Planar images were acquired with a Discovery NM/CT 670 SPECT/CT camera equipped with low-energy high-resolution collimators (image matrix, 512 × 512). Three energy windows were used for image acquisition: standard, 141 keV ± 7.5%; lower, 120 keV ± 5%; and higher, 165 keV ± 5%. A Jaszczak phantom (Jaszczak Flangeless Deluxe SPECT Phantom [Biodex]; cold-rod diameters: 4.8, 6.4, 7.9, 9.5, 11.1, and 12.7 mm; cylinder interior dimensions: Ø 20.4 × 18.6 cm) filled with a solution of ^{99m}Tc-pertechnetate was positioned vertically on top of the camera collimator. Images (1 at each time point) were acquired to reach comparable total numbers of counts for generator-eluted ^{99m}Tc (730 MBq) and cyclotron-produced ^{99m}Tc (620−746 MBq) at 5, 7.5, 9, 11, 13, 15, and 17 h after the end of

TABLE 2
Demographic Data

Method	Participant	Sex	Indication	Age (y)	Body mass index	Administered activity (MBq)	Injection time*	Whole-body imaging time*	Percentage estimated effective dose increase	Imaging findings according to indication
Cyclotron	C1	F	Bilateral thyroid nodule	45	28.0	296.8	5:03	6:34		Hypothyroidism
	C2	F	Hyperthyroidism, Graves disease	49	31.3	351.5	6:31	7:29	1.04	Graves disease
	C3	F	Multinodular goiter	77	25.0	291.4	5:48	7:32	1.20	Subclinical hyperthyroidism
	C4	F	Hypothyroidism	34	19.4	351.0	5:36	6:34	0.94	Thyroiditis
	C5	F	Hyperthyroidism	28	17.2	353.3	6:49	7:52	1.15	Thyroiditis, goiter?
	C6	M	Nodules	60	22.7	329.9	4:54	6:13	1.54	Multinodular goiter
	C7	F	Graves disease	19	25.5	270.7	6:07	7:04	1.75	Graves disease
	C8	M	Hyperthyroidism de novo	65	27.6	330.2	4:40	6:03	1.60	Thyroiditis
	C9	F	Hyperthyroidism	47	35.8	308.6	6:41	7:32	1.98	Graves disease
	C10	F	Thyroiditis or hyperthyroidism	32	34.1	347.7	5:35	6:13	1.76	Thyroiditis
	C11	M	Hyperthyroidism	36	22.6	348.4	7:03	9:00	1.93	Graves disease
Generator	G1	F	Nodule	34	39.8	345.6	NA	NA	NA	Nonfunctional nodule formation
	G2	M	Hyperthyroidism	66	21.1	346.5	NA	NA	NA	Thyroiditis
	G3	F	Goiter, Graves disease	31	24.2	341.7	NA	NA	NA	Subclinical hyperthyroidism, suspected thyroid nodule
	G4	F	Nodules	47	19.7	340.0	NA	NA	NA	Subclinical hyperthyroidism, hyperfunctional nodules
	G5	F	Hyperthyroidism	28	18.3	349.5	NA	NA	NA	Graves disease
	G6	F	Nodules	50	16.2	334.6	NA	NA	NA	Multinodular goiter
	G7	M	Nodule	59	27.2	345.1	NA	NA	NA	Nonfunctional thyroid nodule
	G8	F	Hyperthyroidism	35	35.3	336.0	NA	NA	NA	Graves disease, suspected nonfunctional nodule

*Hours after EOB.
NA = not applicable.

bombardment (EOB). Image contrast and contrast-to-noise ratio (CNR) were calculated with the following equations:

$$\text{Contrast} = \frac{R_{hot} - R_{cold}}{R_{cold}};\ \text{CNR} = \frac{\frac{R_{hot} - R_{cold}}{R_{cold}}}{\sqrt{\left(\frac{\sigma_{hot}}{R_{hot}}\right)^2 + \left(\frac{\sigma_{cold}}{R_{cold}}\right)^2}},$$

where R_i are counts per second per pixel and σ_i are standard deviations. The R_{cold} values were determined by averaging the background count rates in the largest (12.7 mm) cold spots, whereas the R_{hot} values were estimated in a large region of interest surrounding the cold spots.

RESULTS

Provision of ^{99m}Tc-Pertechnetate

Cyclotron-produced ^{99m}Tc-NaTcO$_4$ solutions for injection had a radioactive concentration of 329 ± 84 (mean ± SD) MBq/mL (range, 230−471 MBq/mL), a pH of 5.0−5.5, a radiochemical purity of at least 98%, and a radioisotopic purity of greater than 99.97% (Table 1). All prepared batches complied with standard requirements for parenteral injections, including sterility and endotoxin level.

Patient Demographics and Study Design

The 11 participants injected with cyclotron-produced ^{99m}Tc-NaTcO$_4$ received 325 ± 29 MBq (range, 271−353 MBq). Most

TABLE 3
Results of Selected Biochemical and Hematologic Tests

Analysis	Normal value	Value before injection*	Value after injection*
Alanine aminotransferase			
Men	0–55 IU/L	27 ± 16 (3)	24 ± 17 (3)
Women	0–37 IU/L	23 ± 11 (7)	23 ± 11 (7)
Albumin	35–52 g/L	38 ± 2 (10)	42 ± 2 (10)
Aspartate aminotransferase			
Men	0–40 IU/L	21 ± 8	19 ± 7
Women	0–32 IU/L	22 ± 5	21 ± 6
Bilirubin (total)	2.8–17.0 μmol/L	8.5 ± 6.3	9.4 ± 7.6
Calcium (blood)	2.07–2.55 mmol/L	2.30 ± 0.07	2.27 ± 0.10
Carbon dioxide	23.0–27.0 mmol/L	25.5 ± 2.6	25.6 ± 2.5
Chlorides (blood)	96–106 mmol/L	102 ± 3	103 ± 2
Creatinine (blood)			
Men	58–110 μmol/L	80 ± 27	76 ± 22
Women	46–92 μmol/L	57 ± 10	56 ± 10
γ-glutamyltransferase (serum)			
Men	0–64 IU/L	32 ± 5	33 ± 7
Women	0–55 IU/L	34 ± 21	33 ± 21
Glucose (blood)	3.3–6.1 μmol/L	5.9 ± 1.4	5.4 ± 1.8
Lactate dehydrogenase			
Men	0–250 IU/L	158 ± 13	133 ± 13
Women	0–235 IU/L	154 ± 34	158 ± 30
Alkaline phosphatase			
Men	40–130 IU/L	83 ± 33	82 ± 32
Women	35–105 IU/L	72 ± 30	72 ± 30
Potassium (blood)	3.5–5.1 μmol/L	4.0 ± 0.3	4.2 ± 0.3
Total proteins (blood)	58–80 g/L	69 ± 3	68 ± 3
Sodium (blood)	135–145 μmol/L	140 ± 1	141 ± 2
Urea (blood)			
Men	3.2–7.6 mmol/L	6.1 ± 0.8	6.0 ± 0.8
Women	2.5–6.6 μmol/L	3.9 ± 1.5	3.6 ± 1.5
White blood cells	1×10^9–50×10^9/L	7 ± 1	7 ± 2
Hemoglobin			
Men	130–180 g/L	157 ± 13	155 ± 13
Women	120–160 g/L	132 ± 8	132 ± 7
Platelets	20×10^9–$1{,}000 \times 10^9$/L	235 ± 69	218 ± 74
Cholesterol			
Men	2.81–4.89 mmol/L	3.81 ± 0.38	3.79 ± 0.45
Women	2.69–5.88 mmol/L	4.40 ± 0.64	4.41 ± 0.71
Triglycerides	<1.7 mmol/L	1.6 ± 1.1	1.5 ± 1.0

*Reported as mean ± SD; values in parentheses are numbers of patients.

participants were women (73%). The mean age was 44.7 ± 17.3 y (range, 19−77 y; median, 45 y). The body mass index was 26.3 ± 5.8 (range, 17.2−35.8). Four of the 11 patients had Graves disease, 4 had thyroiditis, and the others had hypothyroidism, subclinical hyperthyroidism, or multinodular goiter. Cyclotron-produced ^{99m}Tc-pertechnetate was administered between 4 h 40 min and 7 h 3 min (280−423 min) after the EOB. On average, the time of injection was approximately 6 h from the EOB.

Eight participants paired by age and sex with the first group were injected with conventional ^{99m}Tc-$NaTcO_4$ and received 342 ± 5 MBq. In this cohort, 75% of the participants were women. The mean age was 43.8 ± 13.9 (range, 28−66; median, 41). The body mass index was 23.8 ± 8.0 (range, 16.2−39.8). By indication, 2 patients had Graves

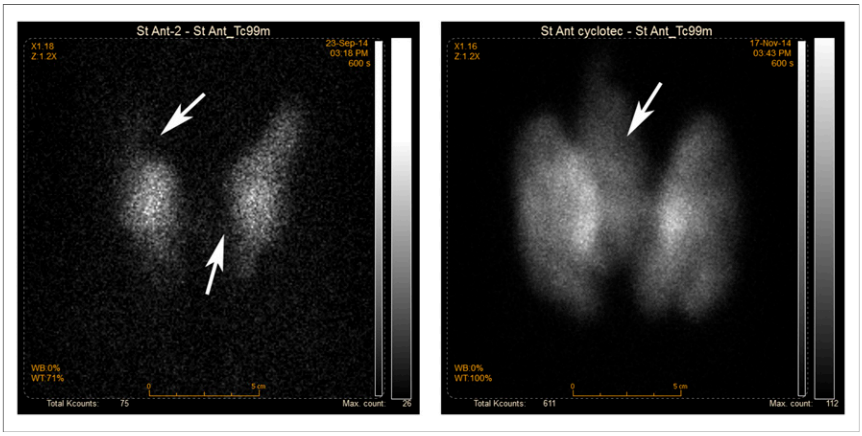

FIGURE 1. Examples of thyroid images obtained with cyclotron-produced ^{99m}Tc-pertechnetate. (Left) Low radioactivity accumulation in cold nodules (arrows) in upper inner right lobe and in isthmus in proximity of left lobe of thyroid gland. (Right) High accumulation in thyroid gland with visible pyramidal lobe (arrow) in presence of hyperthyroidism (Graves disease).

disease, 2 had subclinical hyperthyroidism, 2 had nonfunctional nodules, 1 had multinodular goiter, and 1 had thyroiditis. The patients were not paired by clinical indication.

All patients enrolled in the study completed the trial. Nevertheless, 2 patients did not undergo the entire study protocol because of technical issues. One patient injected with cyclotron-produced ^{99m}Tc-$NaTcO_4$ had an incomplete blood test. Patient demographics are summarized in Table 2.

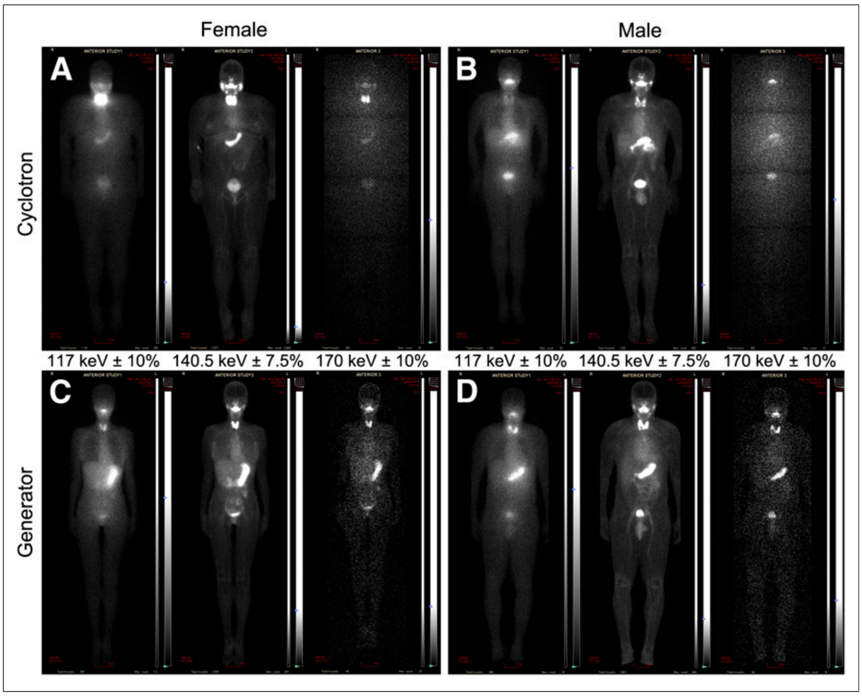

FIGURE 2. Scans obtained for 2 women and 2 men with cyclotron-produced (patient C2 [A] and patient C6 [B]) and generator-eluted (patient G6 [C] and patient G7 [D]) ^{99m}Tc-pertechnetate; anterior images are shown. Visually, image quality in standard-energy window (middle in each quadrant) and in lower-energy window (left in each quadrant) were identical for both radiotracers. Increased uniform background was observed in higher-energy window (right in each quadrant) for cyclotron-produced ^{99m}Tc. Patient data are provided in Table 2.

Safety Evaluation

For cyclotron-produced ^{99m}Tc-$NaTcO_4$, heart rate and blood pressure were within normal limits for all patients and did not change significantly after injection. Hematologic and biochemical test results did not show any significant changes and were well within physiologic values (Table 3). No clinically detectable pharmacologic effects or adverse events were reported during the study.

Dosimetry

On average, the increase in the effective dose over that for ^{99m}Tc-pertechnetate without any radionuclidic impurities was 1.5% ± 0.4%.

Imaging

At the time of imaging, low-level radioactivity was still present in the blood pool. Low-level radioactivity was also observed in the lungs, liver, bone, and soft tissues. The salivary glands, stomach, kidneys, and bladder had the highest uptake among the nontargeted organs, as expected. Tracer uptake in the thyroid varied from weak to strong and was dependent on the underlying pathology, as exemplified by Figure 1. As expected for ^{99m}Tc-pertechnetate, there was no uptake in the brain. The organ distributions were the same for men and women, as shown in representative images (Fig. 2). Among matched patients, the organ distributions were identical for cyclotron-produced ^{99m}Tc-pertechnetate and generator-eluted ^{99m}Tc-pertechnetate (Fig. 3).

Visually, the images acquired in the standard- and lower-energy windows were equivalent for cyclotron-produced ^{99m}Tc-pertechnetate and generator-eluted ^{99m}Tc-pertechnetate. Interpreters were unable to classify the images according to the origin of ^{99m}Tc because of the absence of systematic image features (interobserver κ-value, 0.17; χ^2 test $P = 0.83$). The count rate observed in the higher-energy window increased considerably for the cyclotron-produced ^{99m}Tc-pertechnetate, resulting in a subject's faint silhouette on an almost uniform background (Fig. 2). Because no characteristic γ-rays from contaminants can be identified in the 170 keV ± 10% range, most detected events in the higher-energy window are scatters from high-energy γ-rays. The high uniform background in the higher-energy window suggests the same.

Image Analysis

The ratios of counts in the lower-energy window to those in the standard-energy window were comparable for the cyclotron-produced radiotracer (59% ± 2%) and the generator-eluted radiotracer (54% ± 4%). The ratios of counts in the higher-energy window to those in the standard-energy window were significantly higher for cyclotron-produced ^{99m}Tc-pertechnetate (15% ± 3% vs. 4% ± 1%), in accordance

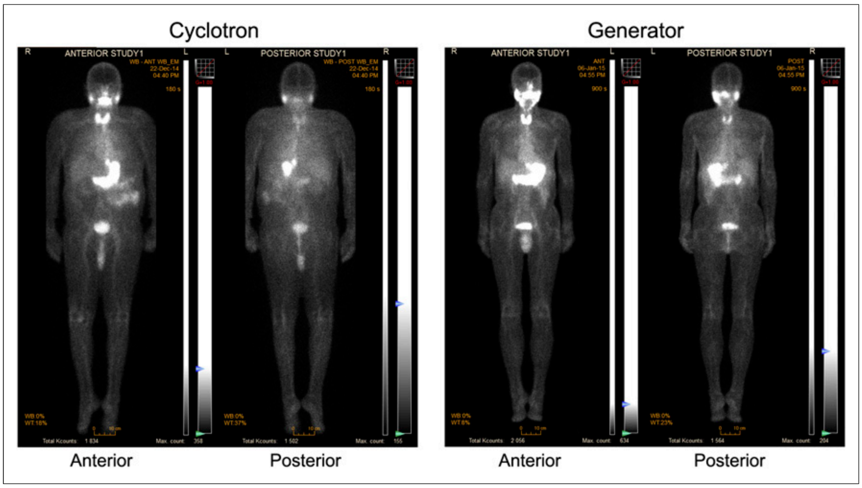

FIGURE 3. Scans obtained for 2 men, both with thyroiditis, with cyclotron-produced (patient C8 [left]) and generator-eluted (patient G2 [right]) ^{99m}Tc-pertechnetate. Images acquired in standard-energy window were visually equivalent in terms of expected biodistribution of tracer as well as image quality.

with the visual image interpretation (Fig. 2). Data for individual study participants are shown in Table 4. Count ratios in the higher-energy window (170 keV ± 10%) were consistent with the expected buildup of longer-lived ^{96}Tc (Fig. 4).

TABLE 4

Ratios of Counts in Lower- and Higher-Energy Windows to Those in Standard-Energy Window for Individual Patients

		Anterior–posterior geometric mean ratio*	
Method	Participant	Lower/standard	Higher/standard
Cyclotron	C1	58	18
	C2	59	11
	C3	56	13
	C4	60	10
	C5	55	11
	C6	57	15
	C7	59	16
	C8	59	16
	C9	63	18
	C10	62	17
	C11	58	17
Generator	G1	59	3
	G2	51	5
	G3	56	6
	G4	54	3
	G5	53	3
	G6	51	3
	G7	55	3
	G8	57	4

*Reported as percentages.

Phantom Imaging

Phantom imaging data (Fig. 5) were in agreement with the information derived from patients' scans. We observed an increase in the ratio of counts in the higher-energy window from 2% with generator-derived ^{99m}Tc to 4%−10% with cyclotron-produced ^{99m}Tc, and this increase was dependent on the time elapsed after the EOB (Fig. 6). Nevertheless, the contrast and contrast-to-noise ratio in the standard-energy window remained stable over the course of the experiment (up to 18 h after irradiation) (Fig. 6).

DISCUSSION

The main feature distinguishing cyclotron-produced ^{99m}Tc from generator-eluted ^{99m}Tc is the presence of other technetium isotopes (Table 1) that may contribute to additional radiation doses for patients and affect image quality. The radioisotopic purity of ^{99m}Tc-pertechnetate produced with a cyclotron at medium energies (20−24 MeV) was previously evaluated, and the quality of the final formulation was confirmed to be fully adequate for clinical use, provided that the isotopic composition of the starting molybdenum and its irradiation parameters (energy and time) were appropriately selected (*7*). Although the radiochemical entity in the cyclotron-produced formulation (^{99m}Tc-pertechnetate) was the same as that in the generator-eluted formulation, the raw materials and chemical reagents used for manufacturing were different. Therefore, the cyclotron-produced radiopharmaceutical formulation needed to be assessed for safety for human use, and its imaging efficacy needed to be confirmed in a clinical study with a limited number of patients.

Eleven patients were successfully imaged with cyclotron-produced ^{99m}Tc-pertechnetate. The injection was well tolerated, and the patients did not report any discomfort due to tracer administration. The safety evaluation results did not indicate any alterations in sequential blood values and vital signs.

All technetium isotopes are chemically equivalent and have the same biologic retention and distribution characteristics. For the

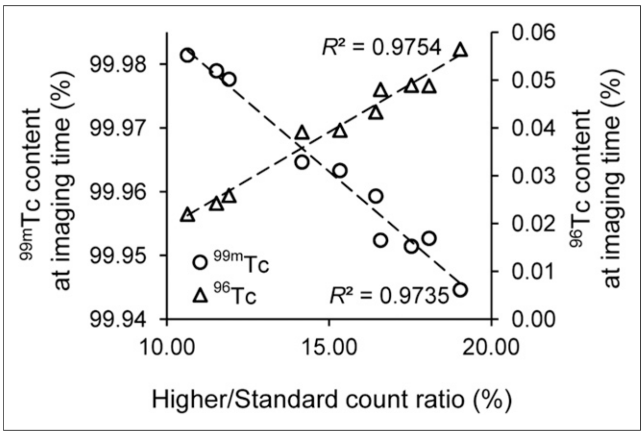

FIGURE 4. Steady increase in ratios of counts in higher-energy window to those in standard-energy window with expected buildup of longer-lived ^{96}Tc.

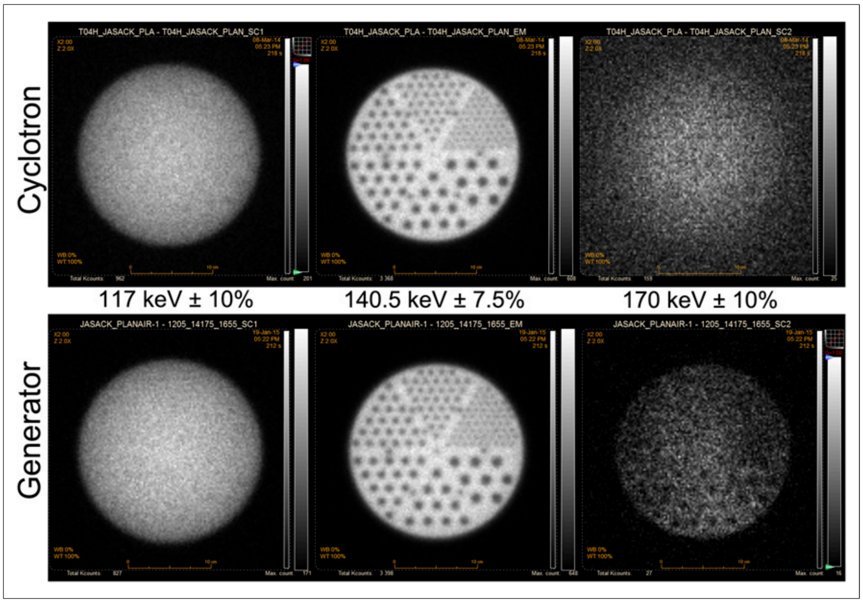

FIGURE 5. Typical phantom images obtained with cyclotron-produced (9 h after EOB; 723 MBq [top]) and generator-eluted (730 MBq [bottom]) ^{99m}Tc. Images are on linear gray scale, with white representing maximum intensity. Cold rods were 4.8, 6.4, 7.9, 9.5, 11.1, and 12.7 mm in diameter.

purpose of effective dose estimation, however, the actual residence time depends on the physical half-life of each isotope. In addition, the particle emission profile and energy are different for individual isotopes. Therefore, the tissue-to-organ absorbed doses vary for each technetium isotope. Since the relative proportions of technetium isotopes in a formulation change with time because of their distinct decay characteristics, the radioisotopic content of the product at the time of intravenous administration must be used to estimate patients' doses. The obtained values, expressed as a percentage dose increase compared with ^{99m}Tc without any radionuclidic impurities (Fig. 7), fitted well with our previous calculations (*7*). The estimated effective dose increase observed in the present study was minimal and well below the postulated acceptable limit of 10%.

^{99m}Tc eluted from generators also contains radionuclidic impurities (*9–11*), but their contributions are not accounted for in a dose assessment because biokinetic data are not available for all nuclides or their corresponding radioactive chemical species. Recently, another group used a theoretic model to investigate the influence of the isotopic composition of starting molybdenum on a potential dose increase for patients and suggested thresholds for isotopic contamination of initial ^{100}Mo by other Mo isotopes (*12*).

As expected, the whole-body images confirmed the normal distribution of ^{99m}Tc-pertechnetate in the thyroid, salivary glands, stomach, and urinary bladder. A comparative assessment of images of paired participants also showed this finding (Figs. 2 and 3). Images of the thyroid also correlated well with the underlying pathology (Fig. 1; Table 2); these data provided supporting evidence of the suitability of cyclotron-produced ^{99m}Tc-pertechnetate for diagnostic clinical use.

No particular characteristics were noted when the 2 nuclear medicine specialists were asked to determine which patients were injected with cyclotron-produced pertechnetate. Clinically, the images were of similar quality and showed similar biodistributions. Impurities present in the cyclotron formulation did not create any clinically relevant features on images obtained in the standard-energy window.

Quantitatively, for cyclotron-produced ^{99m}Tc, the ratio of counts increased by approximately 9% in the lower-energy window (from 54% ± 4% to 59% ± 2%). At the same time, a 4-fold increase (from 4% ± 1% to 15% ± 3%) was observed in the higher-energy window (Table 4). Nonetheless, despite the increased background in adjacent energy windows, trace amounts of isotopic impurities present in cyclotron-produced ^{99m}Tc did not affect in any significant way the image definition in the standard-energy window. As demonstrated with phantoms earlier (*7*) and in the present study (Figs. 5 and 6), the spatial resolution and contrast in the standard-energy window remained comparable for both cyclotron-produced ^{99m}Tc and generator-eluted ^{99m}Tc. Theoretic simulations support these findings (*13*). Therefore, the effect that may be due to scattering of high-energy γ-rays originating from isotopic contaminants such as ^{94}Tc, ^{94m}Tc, and ^{96}Tc can be considered negligible as long as the product meets radionuclidic purity specifications based on dosimetry considerations or product shelf-life, whichever is shorter.

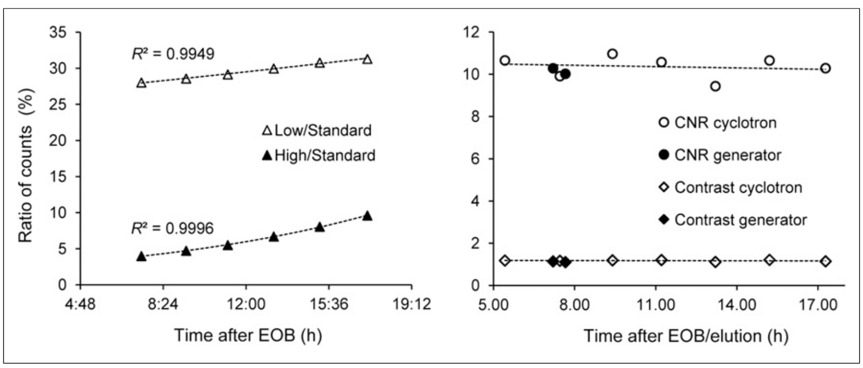

FIGURE 6. (Left) Ratios of counts in lower- and higher-energy windows to those in standard-energy window as function of time. (Right) Contrast and contrast-to-noise ratio (CNR) in standard-energy window as function of time.

The production of ^{99m}Tc with cyclotrons is a reiterated idea (*14*) that received little attention before the ongoing supply of inexpensive and readily available ^{99m}Tc from ^{99}Mo generators became uncertain. In recent years, several groups, including our consortium, developed new targets and robust separation procedures to manufacture high-purity ^{99m}Tc with cyclotrons (*7,15–20*). There is increasingly convincing evidence that the quality of cyclotron-produced ^{99m}Tc is comparable to that of conventional ^{99m}Tc (*6,7,21,22,23*) and that sufficient quantities can be made to satisfy the demand of large urban communities (*3*).

The present clinical trial confirmed that cyclotron-produced ^{99m}Tc-pertechnetate

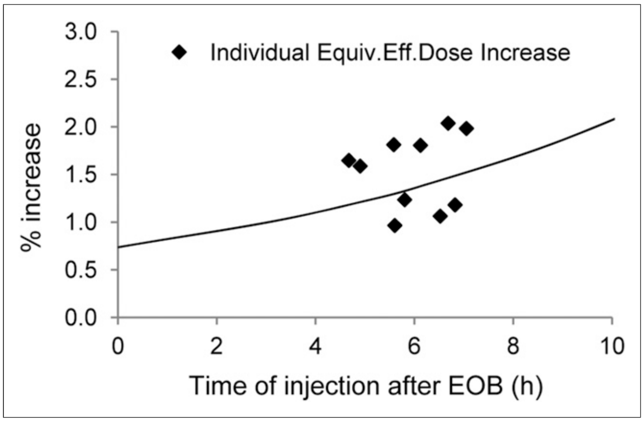

FIGURE 7. Estimated equivalent (Equiv.) effective (Eff.) dose increase for each patient injected with cyclotron-produced ^{99m}Tc. Solid line shows predicted radiation dose increase (*7*).

provides clinical safety and diagnostic efficacy equivalent to those of the conventional radiopharmaceutical. Whether cyclotron-produced ^{99m}Tc will reach the status of an approved radiopharmaceutical or be forgotten again remains to be seen. Although the cost of its commercialization (infrastructure and marketing authorization) may be orders of magnitude lower than that of nuclear reactor–based production of ^{99m}Tc, it is still significant and will require commitment from governments and investors. Economic factors, including the implementation of full-cost recovery models for ^{99}Mo/^{99m}Tc production (*2*), will be a decisive point in this almost 50-y-old story.

CONCLUSION

We showed that ^{99m}Tc produced with a cyclotron at medium energy can be safely used for humans and yields clinical images that are fully satisfactory for diagnostic procedures. The results of the present study provide further supporting evidence for the adoption of cyclotron-produced ^{99m}Tc-pertechnetate in clinical practice.

DISCLOSURE

This work was supported by Natural Resources Canada through the Isotope Technology Acceleration Program (ITAP) and by the Medical Imaging Trial Network of Canada (MITNEC). The Research Center of CHUS (CRCHUS) is supported by the Fonds de Recherche du Québec–Santé (FRQS). No other potential conflict of interest relevant to this article was reported.

ACKNOWLEDGMENTS

We gratefully acknowledge Jim Garrett, Laboratory of Materials Preparation and Characterization, Brockhouse Institute for Materials Research, McMaster University, for preparing ^{100}Mo targets. We thank cyclotron operators Eric Berthelette and Paul Thibault for excellent technical help and continuing availability for this research project and Otman Sarrhini for phantom image analysis. We acknowledge our ITAP partners, University of Alberta and Advanced Cyclotron Systems Inc.

REFERENCES

1. Rahmim A, Zaidi H. PET versus SPECT: strengths, limitations and challenges. *Nucl Med Commun.* 2008;29:193–207.
2. Organisation for Economic Co-operation and Development, Nuclear Energy Agency. Full-cost recovery for molybdenum-99 irradiation services: methodology and implementation. Guidance document NEA/SEN/HLGMR(2012)9. http://www.oecd-nea.org/med-radio/guidance/docs/full-cost-recovery-molybdenum-99-irradiation.pdf. Published February 2012. Accessed November 23, 2016.
3. Bénard F, Buckley KR, Ruth TJ, et al. Implementation of multi-Curie production of ^{99m}Tc by conventional medical cyclotrons. *J Nucl Med.* 2014;55:1017–1022.
4. McEwan A, McQuarrie S, Abrams D, et al. Technetium-99m (Tc-99m) pertechnetate (TcO_4) imaging with cyclotron produced Tc-99m compared with generator Tc-99m [abstract]. *J Nucl Med.* 2012;53(suppl 1):1487.
5. Celler A, Hou X, Bénard F, Ruth T. Theoretical modeling of yields for proton induced reactions on natural and enriched molybdenum targets. *Phys Med Biol.* 2011;56:5469–5484.
6. Lebeda O, van Lier EJ, Štursa J, Ráliš J, Zyuzin A. Assessment of radionuclidic impurities in cyclotron produced ^{99m}Tc. *Nucl Med Biol.* 2012;39:1286–1291.
7. Selivanova SV, Lavallée É, Senta H, et al. Radioisotopic purity of sodium pertechnetate ^{99m}Tc produced with a medium-energy cyclotron: implications for internal radiation dose, image quality, and release specifications. *J Nucl Med.* 2015;56:1600–1608.
8. McAlister DR, Horwitz EP. Automated two column generator systems for medical radionuclides. *Appl Radiat Isot.* 2009;67:1985–1991.
9. Monograph 124: sodium pertechnetate (^{99m}Tc) injection (fission). In: *European Pharmacopoeia.* 5th ed. Strasbourg, France: Council of Europe; 2005:847–848.
10. Monograph 283: sodium pertechnetate (^{99m}Tc) injection (non-fission). In: *European Pharmacopoeia.* 5th ed. Strasbourg, France: Council of Europe; 2005:848–849.
11. United States Pharmacopeial Convention, Official Monographs: USP32–NF27 Page 3669, Sodium Pertechnetate Tc 99m Injection, 2010.
12. Hou X, Tanguay J, Buckley K, et al. Molybdenum target specifications for cyclotron production of ^{99m}Tc based on patient dose estimates. *Phys Med Biol.* 2016;61:542–553.
13. Hou X, Tanguay J, Benard F, et al. Investigation of the impact on image resolution of trace impurities found in cyclotron-produced Tc pertechnetate [abstract]. *J Nucl Med.* 2015;56(suppl 3):1749.
14. Beaver JE, Hupf H. Production of ^{99m}Tc on a medical cyclotron: a feasibility study. *J Nucl Med.* 1971;12:739–741.
15. Targholizadeh H, Raisali G, Jalilian AR, Rostampour N, Ensaf M, Dehghan MK. Cyclotron production of technetium radionuclides using a natural metallic molybdenum thick target and consequent preparation of [Tc]-BRIDA as a radiolabelled kit sample. *Nukleonika.* 2010;55:113–118.
16. Morley TJ, Dodd M, Gagnon K, et al. An automated module for the separation and purification of cyclotron-produced $^{99m}TcO_4^-$. *Nucl Med Biol.* 2012;39:551–559.
17. Gagnon K, Wilson JS, Holt CMB, et al. Cyclotron production of ^{99m}Tc: recycling of enriched ^{100}Mo metal targets. *Appl Radiat Isot.* 2012;70:1685–1690.
18. Wild D, Wilson J, Thomas B, et al. Tentagel as chromatography media for processing cyclotron produced ^{99m}Tc [abstract]. *J Nucl Med.* 2014;55(suppl 1):1248.
19. Hanemaayer V, Benard F, Buckley KR, et al. Solid targets for ^{99m}Tc production on medical cyclotrons. *J Radioanal Nucl Chem.* 2014;299:1007–1011.
20. Bénard F, Zeisler SK, Vuckovic M, et al. Cross-linked polyethylene glycol beads to separate ^{99m}Tc-pertechnetate from low-specific-activity molybdenum. *J Nucl Med.* 2014;55:1910–1914.
21. Guérin B, Tremblay S, Rodrigue S, et al. Cyclotron production of ^{99m}Tc: an approach to the medical isotope crisis. *J Nucl Med.* 2010;51(4):13N–16N.
22. Rovais MRA, Aardaneh K, Aslani G, Rahiminejad A, Yousefi K, Boulouri F. Assessment of the direct cyclotron production of ^{99m}Tc: an approach to crisis management of ^{99m}Tc shortage. *Appl Radiat Isot.* 2016;112:55–61.
23. Das MK, Madhusmita, Chattopadhyay S, et al. Production and separation of ^{99m}Tc from cyclotron irradiated $^{100/natural}$Mo targets: a new automated module for separation of ^{99m}Tc from molybdenum targets. *J Radioanal Nucl Chem.* 2016;310:423–432.